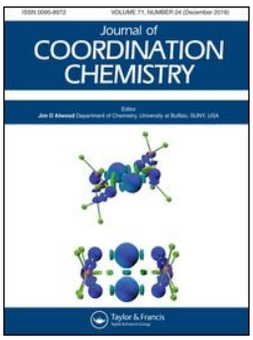

Taylor & Francis
Taylor & Francis Group

Journal of Coordination Chemistry

ISSN: 0095-8972 (Print) 1029-0389 (Online) Journal homepage: https://www.tandfonline.com/loi/gcoo20

Aarene platinum group metal complexes containing imino-quinolyl ligands: synthesis and antibacterial studies

Agreeda Lapasam, Sanjay Adhikari, Venkanna Banothu, Uma Addepally & Mohan Rao Kollipara

To cite this article: Agreeda Lapasam, Sanjay Adhikari, Venkanna Banothu, Uma Addepally & Mohan Rao Kollipara (2020): Aarene platinum group metal complexes containing imino-quinolyl ligands: synthesis and antibacterial studies, Journal of Coordination Chemistry, DOI: 10.1080/00958972.2020.1753037

To link to this article: https://doi.org/10.1080/00958972.2020.1753037

JOURNAL OF COORDINATION CHEMISTRY
https://doi.org/10.1080/00958972.2020.1753037

Taylor & Francis
Taylor & Francis Group

Aarene platinum group metal complexes containing imino-quinolyl ligands: synthesis and antibacterial studies

Agreeda Lapasam[a], Sanjay Adhikari[a], Venkanna Banothu[b], Uma Addepally[b] and Mohan Rao Kollipara[a]

[a]Centre for Advanced Studies in Chemistry, North Eastern Hill University, Shillong, India; [b]Centre for Biotechnology (CBT), Institute of Science & Technology (IST), Jawaharlal Nehru Technological University Hyderabad (JNTUH), Hyderabad, India

ABSTRACT

Imino-quinolyl Schiff-base ligands have been prepared by the condensation reaction of substituted 2-aminopyridine and quinoline-2-carbaldehyde. The reaction of $[(arene)MCl_2]_2$ with imino-quinolyl Schiff-base ligands leads to the formation of cationic complexes $[(arene)M(L)Cl]^+$ (**1**–**12**). Single crystal X-ray diffraction studies were used to confirm the coordination mode and structures of these complexes. The molecular structures of these complexes revealed that they adopt characteristic three-legged piano stool geometry with the metal coordinating through a terminal chloride and imino-quinolyl ligands in a bidentate chelating NN′ fashion. The ligand coordinates to the metal center through the nitrogen of the quinoline and the imine nitrogen forming a five-membered metallacycle. These compounds were evaluated for their *in vitro* antibacterial activity by the agar well diffusion method against *Staphylococcus aureus*, *Escherichia coli* and *Klebsiella pneumoniae* strains. Results show that all the ligands and complexes inhibited the growth of bacteria.

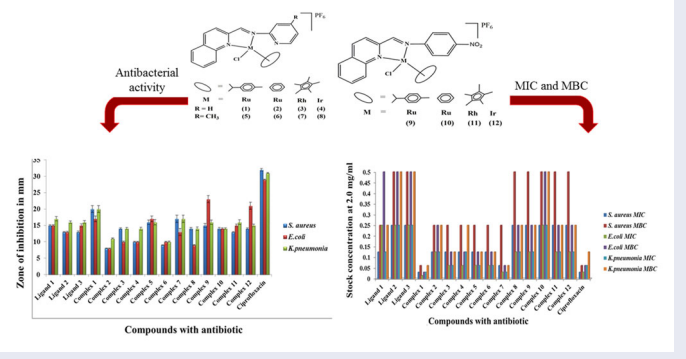

ARTICLE HISTORY

Received 12 November 2019
Accepted 27 March 2020

KEYWORDS

Ruthenium; rhodium; iridium; imino-quinolyl; antibacterial activity

CONTACT Mohan Rao Kollipara mohanrao59@gmail.com Centre for Advanced Studies in Chemistry, North Eastern Hill University, Shillong, 793022, India.

Supplemental data for this article is available online at https://doi.org/10.1080/00958972.2020.1753037.

1. Introduction

One of the major advances in medical science over the last century has been the development of antimicrobials. Due to challenges that current drugs face today, the development of significant antibacterial compounds remains one of the attractive areas. Drug-resistant pathogens have become an important cause of morbidity and mortality worldwide; methicillin-resistant *Staphylococcus aureus*, vancomycin-resistant *Enterococcus*, and fluoroquinolone resistant *Pseudomonas aeruginosa* show rapidly increasing incidence of infection with treatment failure leading to high mortality rates [1]. Extensive attention has been paid to the chemistry of half-sandwich organometallic complexes because of their broad spectrum in biological and medicinal fields [2–5]. Ruthenium complexes of organic drugs can overcome resistance developed by the microbe to the organic compound alone as ruthenium offers numerous advantages including low micromolar potency, scope of controlling the shape and the chemical and pharmacological properties of the complex by the abundant selection of the arene and the ligands at the "legs" of the "piano-stool" structure [6]. Ruthenium complexes show some potential against drug-resistant bacterial strains, including examples of Ru – polypyridyl complexes and RAPTA-type complexes showing promising antibacterial activity [7]. Ruthenium mononuclear complexes have shown good antibacterial activity, particularly against Gram-positive bacteria. Dinuclear ruthenium complexes appear to show greater potential as their activity is generally maintained against antibiotic-resistant bacterial strains [8]. Binuclear rhodium(II) complexes $[Rh_2(OOCR)_2(N\text{-}N)_2(H_2O)_2]^{2+}$ (N-N = bi-py, phen.) are effective antibacterial and antitumor agents [9, 10]. Syntheses of organoiridium(III) complexes have given rise to a broad range of biological activities such as antiproliferative, antibacterial activity and the delocalization of the π-electrons over the chelate ring helps to increase the lipophilicity of the complexes and enables their penetration into bacterial cell membranes, hence hindering the growth of bacteria [11].

Quinoline (nitrogen-containing heterocycle) and its derivatives represent a class of organic compounds having wide optical and bioactive properties. Large varieties of quinoline core moieties can be repeatedly found in the structure of several naturally occurring alkaloids. They have been correlated with a wide range of biological activities including malaria, bacterial infection and tuberculosis [12]. A quinoline based ligand has been employed as a fluorescent probe of Ag^+ ion in aqueous media [13]. Transition metal complexes of quinoline have also displayed their remarkable activity as catalysts towards polymerization reactions [14]. Organoruthenium complexes of 8-hydroxy quinoline have been reported which possess excellent anticancer properties, thus making these complexes potential candidates as anticancer drugs [15].

Our group has reported many half-sandwich metal complexes bearing Schiff-base ligands with interesting coordination modes of the ligands [16, 17]. Stimulated by the success of both Schiff base and ruthenium complexes in biological activity, we have combined both types to prepare arene metal complexes bearing an imino-quinolyl Schiff base ligand. Keeping our interest with Schiff base ligands, herein we report the synthesis, structural and biological aspects of 12 new conformationally rigid organometallic half-sandwich complexes synthesized by the reaction of precursor complexes

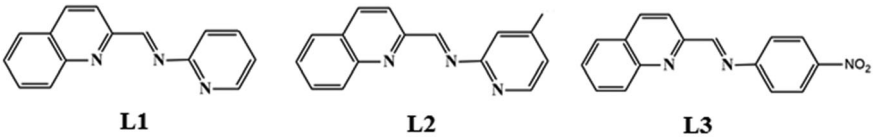

Chart 1. Ligands used in the present study.

with ligands in 1:2 ratios in the presence of ammonium hexafluorophosphate. Chart 1 represents the ligands used in the present study.

2. Experimental

2.1. Physical methods and materials

All reagents were purchased from commercial sources and used as received without purification. 2-Quinolinecarboxaldehyde, 4-nitroaniline, and 2-aminopyridine were obtained from Sigma-Aldrich. The solvents were purified and dried according to standard procedures [18]. All reactions were carried out under normal conditions. All gram-positive and gram-negative bacterial strains used were obtained from the Department of Microbiology, Osmania General Hospital, Hyderabad. The starting precursor metal complexes $[(p\text{-cymene})RuCl_2]_2$, $[(benzene)RuCl_2]_2$, and $[Cp^*MCl_2]_2$ (M = Rh/Ir) were prepared according to the literature methods [19, 20]. Infrared spectra were recorded on a Perkin-Elmer 983 spectrophotometer by using KBr pellets from 400 to 4000 cm^{-1}. ^1H NMR spectra were recorded on a Bruker Avance II 400 MHz spectrometer using DMSO-d_6 and $CDCl_3$ as solvents. Absorption spectra were recorded on a Perkin-Elmer Lambda 25 UV/Visible spectrophotometer from 200 to 600 nm at room temperature in acetonitrile. Mass spectra of **2**–**4** were recorded using a Q-Tof APCI-MS instrument (model HAB 273). Mass spectra of **7**, **8**, **9**, **11** and **12** were recorded using an Agilent 6540 UHD Accurate-Mass Q-TOF LC/MS instrument. Elemental analyses of the c were performed on a Perkin-Elmer 2400 CHN analyzer.

2.2. Single-crystal X-ray structure analyses

Suitable single crystals of **1**, **2** and **4** were obtained by slow diffusion of hexane into acetone or dichloromethane solution. Single crystal X-ray diffraction data for the complexes were collected on an Oxford Diffraction Xcalibur Eos Gemini diffractometer at 293 K using graphite monochromated Mo-Kα radiation ($\lambda = 0.71073$ Å). The strategy for the data collection was evaluated using the CrysAlisPro CCD software. Crystal data were collected by standard "phi–omega scan" techniques and were scaled and reduced using CrysAlisPro RED software. The structures were solved with SHELXT-2016 [21] solution program using the direct method and refined full-matrix least-squares with SHELXL-2016/SHELXL-2018/3 refining on F^2 [22]. Software packages used: CrysAlisPRO for data collection, for cell refinement, data reduction and absorption correction [23]. The positions of all atoms were obtained by direct methods. Metal ions in the complex were located from the e-maps and non-hydrogen atoms were refined anisotropically. Crystallographic and

Table 1. Crystal data and structure refinement details of **1** and **2**.

	1	2
Empirical formula	$C_{50}H_{50}Cl_2F_{12}N_6P_2Ru_2$	$C_{21}H_{17}ClF_6RuN_3P$
Formula weight	1297.94	592.87
Temperature (K)	275(2)	294(2)
Wavelength (Å)	0.71073	0.17073
Crystal system	Triclinic	Monoclinic
Space group	*P* 1	*P21/c*
a (Å)/α (°)	8.9599(4)/77.655(4)	7.1052(3)/90
b (Å)/β (°)	13.7443(5)/86.070(4)	22.6904(11)/98.371(4)
c (Å)/γ (°)	21.5051(11)/85.436(3)	13.7378(7)/90
Volume ($Å^3$)	2575.3(2)	2191.21(18)
Z	2	4
Density (calc) (Mg/m^{-3})	1.674	1.797
Absorption coeff. (μ) (mm^{-1})	0.839	0.976
F(000)	1304	1176
Crystal size (mm^3)	0.25 × 0.11 × 0.09	0.26 × 0.23 × 0.15
Theta range for data collection (°)	3.041 to 29.040	3.08 to 29.03
Index ranges	−11<=h<=10, −18<=k<=16, −29<=l<21	−9<=h<=6, −28<=k<=30, −18<=l<14
Reflections collected	13601	8434
Independent reflections	10645 [R(int) = 0.0233]	4991 [R(int) = 0.0343]
Completeness to theta = 25.00°	93.5%	99.6%
Absorption correction	Semi-empirical from equivalents	Semi-empirical from equivalents
Refinement method	Full-matrix least-squares on F^2	Full-matrix least-squares on F^2
Data/restraints/parameters	10645/0/667	4991/0/298
Goodness-of-fit on F^2	1.022	1.059
Final R indices [I > 2sigma(I)]	R1 = 0.0483, wR2 = 0.1102	R1 = 0.0453, wR2 = 0.0917
R indices (all data)	R1 = 0.0715, wR2 = 0.1242	R1 = 0.0667, wR2 = 0.1032
Largest diff. peak and hole ($e.Å^{-3}$)	0.872 and −0.616	0.527 and −0.600
CCDC No.	1953782	1953783

Structures were refined on F_0^2: $wR_2 = [\Sigma[w(F_0^2 - F_c^2)^2]/\Sigma w(F_0^2)^2]^{1/2}$, where $w^{-1} = [\Sigma(F_0^2)+(aP)^2+bP]$ and $P = [\max(F_0^2, 0)+2F_c^2]/3$.

structure refinement parameters for the complexes are summarized in Table 1, and selected bond lengths and angles are presented in Table 2. The molecular structures of the complexes are presented as thermal ellipsoid plots in Figures 1 and 2 [24].

2.3. Antibacterial activity

An agar-well diffusion method was employed for the evaluation of antibacterial activities of test compounds [25, 26]. All gram-positive and gram-negative bacterial strains used in the present study were obtained from the Department of Microbiology, Osmania General Hospital, Hyderabad. All strains were tested for purity by standard microbiological methods. The bacterial stock cultures were maintained on Mueller-Hinton agar slants and stored at 4 °C. An agar-well diffusion method was employed for the evaluation of antibacterial activities of test compounds. DMSO was used as a negative control. The bacterial strains were reactivated from stock cultures by transferring into Mueller-Hinton broth and incubating at 37 °C for 18 h. A final inoculum containing 106 colonies forming units (1 × 106 CFU/ml) was added aseptically to MHA medium and poured into sterile petri dishes. Different test compounds at a concentration of 200 μg per well were added to the wells (8 mm in diameter). Plates were incubated overnight at 37 °C and the zone of inhibition was measured by considering the diameter around each well (mm). Experiments were performed in triplicate.

Table 2. Selected bond lengths (Å) and angles (°) of **1** and **2**.

	1	2
M1-CNT	1.695	1.688
M1-N1	2.118(4)	2.127(3)
M1-N2	2.085(4)	2.075(3)
M1-Cl1	2.392(1)	2.378(9)
N1-M1-N2	76.6(1)	76.6(1)
N1-M1-Cl1	85.7(1)	84.24(8)
N2-M1-Cl1	87.3(1)	86.99(8)

CNT represents the centroid of the arene ring (arene = p-cymene, benzene) and M = Ru.

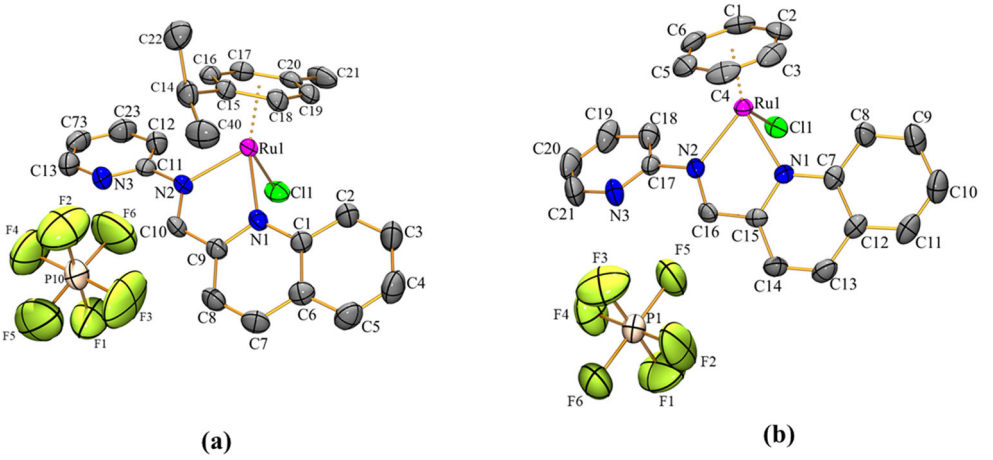

Figure 1. (a) Thermal ellipsoid plot of **1**. (b) Thermal ellipsoid plot of **2** with 50% probability. Hydrogens are omitted for clarity.

2.4. MIC and MBC

The minimum inhibitory concentration (MIC) and minimum bactericidal concentration (MBC) were determined according to a standard protocol [27]. The minimum inhibitory concentration (MIC) and minimum bactericidal concentration (MBC) was determined by the micro-broth dilution method done in 96 well plates according to standard protocol. A 2-fold serial dilution of the compounds, with the appropriate antibiotic, was prepared. Initially, 100 µl of MH broth was added to each well plate. Then 100 µl of compound or antibiotic was taken from the stock solution and dissolved in the first well plate. Serial dilution was done to obtain different concentrations. The stock concentrations of 2.0 mg/ml 24-hour culture turbidity were adjusted to match 0.5 McFarland standards which correspond to 1×108 CFU/ml. The standardized suspension (100 µl) of bacteria was added to all the wells except the antibiotic control well and the 96 well plates were incubated at 37 °C for 24 h. After 24 h of incubation, 40 µl of MTT (3-(4,5-dimethylthiazol-2-yl)-2,5-diphenyltetrazolium bromide) reagent (0.1 mg/ml in 1x PBS) was added to all the wells. MIC was taken as the lowest concentration, which did not show any growth, which was visually noted from the blue color, developed by MTT. Subcultures were made from clear wells and the lowest concentration that yielded no growth after subculturing was taken as the MBC.

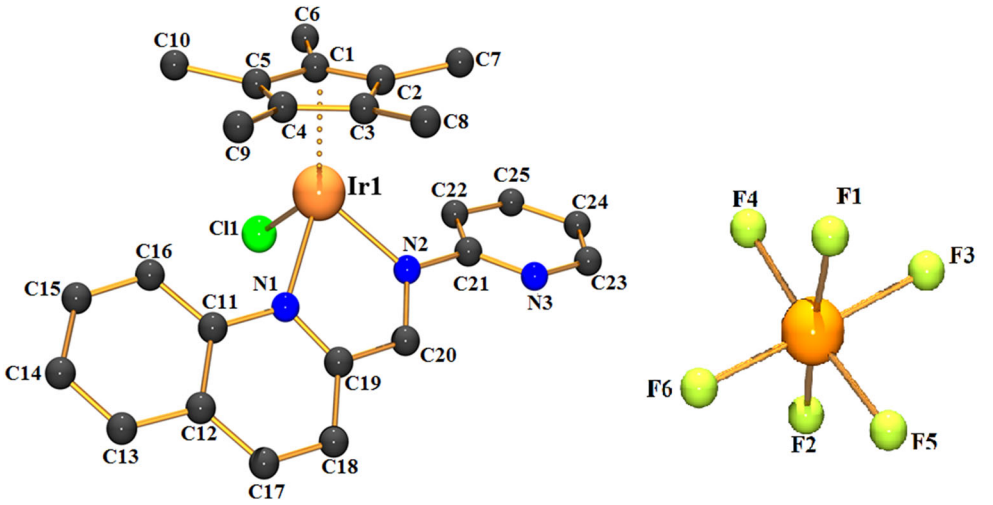

Figure 2. Ball and stick plot of **4**. Hydrogens are omitted for clarity. This complex crystallized in monoclinic system with the following unit cell a = c = 90°, b = 108.467(8), α = 12.0587(11), β = 14.9542(10) and γ = 15.2979(11). Because of the disorder in the crystal the structure of this complex presented here to only confirm the composition of molecule.

2.5. Synthesis of imino-quinolyl ligands

The imino-quinolyl Schiff base ligands L1 and L2 were prepared by the reaction of quinoline-2-carbaldehyde (471.5 mg, 3.000 mmol) and the desired substituted 2-aminopyridine (282.4 mg, 3.000 mmol (L1), 324.5 mg, 3.000 mmol (L2)). Ligand L3 was prepared by condensation of quinoline-2-carbaldehyde (471.5 mg, 3.0 mmol) and 4-nitroaniline (414.5 mg, 3.001 mmol). Quinoline-2-carbaldehyde was dissolved in 10 ml of ethanol to this solution, added substituted 2-aminopyridine or 4-nitroaniline and this reaction mixture was heated under reflux for 24 h. The solvent was evaporated under reduced pressure; the product was obtained and used without further purification (Scheme 1).

2.6. General procedure for preparation of imino-quinolyl metal complexes 1–12

A mixture of metal precursor $[(arene)RuCl_2]_2$ {arene = *p*-cymene (61.2 mg, 0.100 mmol), benzene (50.0 mg, 0.099 mmol)} or $[Cp^*MCl_2]_2$ {M = Rh (61.8 mg, 0.099 mmol)/Ir (79.7 mg, 0.100 mmol) and imino-quinolyl ligand {L1 (46.6 mg) L2 (49.4 mg) L3 (55.4 mg)} (0.200 mmol) was dissolved in dry methanol (5 ml) and stirred at room temperature for 1 h. Then 5 equivalents of NH_4PF_6 dissolved in dry methanol (2 ml) was added dropwise to the reaction mixture and stirring continued for a further 5–6 h whereupon a yellow, red or brown solid precipitated out from the reaction mixture (Scheme 2). The precipitate was collected by filtration, washed with cold methanol and diethyl ether and air dried.

2.6.1. [(P-cymene)Ru(L1)Cl]PF_6 (1)

Red solid, Yield: 44.2 mg (68%); IR (KBr, cm^{-1}): 3447(m), 1590(m), 1568(m), 1462(m), 1437(m), 845(s); ^1H NMR (400 MHz, $CDCl_3$, ppm): 8.98 (s, 1H, $CH_{(imine)}$), 8.60 (d, 1H,

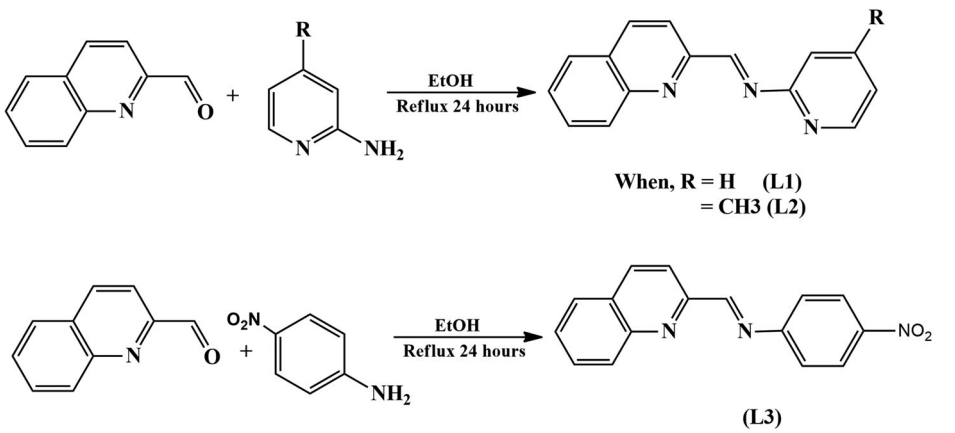

Scheme 1. Synthesis of L1-L3.

$J = 12$ Hz), 8.52 (d, 1H, $J = 4$ Hz), 8.46 (d, 1H, $J = 8$ Hz), 8.10 (d, 1H, $J = 8$ Hz), 7.91–8.00 (m, 3H), 7.86 (t, 1H, $J = 8$ Hz), 7.77 (t, 1H, $J = 8$ Hz), 7.40 (t, 1H, $J = 4$ Hz), 5.69 (d, 1H, $J = 4$ Hz, $CH_{(p\text{-cym})}$), 5.59 (dd, 2H, $J = 4$ and 4 Hz, $CH_{(p\text{-cym})}$), 5.26 (d, 1H, $J = 8$ Hz, $CH_{(p\text{-cym})}$), 2.27 (sept, 1H, $CH_{(p\text{-cym})}$), 2.11 (s, 3H, $CH_{(p\text{-cym})}$), 0.86 (d, 3H, $J = 8$ Hz, $CH_{(p\text{-cym})}$), 0.73 (d, 3H, $J = 8$ Hz, $CH_{(p\text{-cym})}$); ^{13}C NMR (100 MHz, $CDCl_3$, ppm): 167.04, 159.87, 154.34, 148.96, 148.74, 140.54, 139.14, 133.44, 130.62, 129.30, 128.94, 128.22, 125.56, 124.38, 118.76, 106.13, 105.37, 86.01, 85.85, 84.63, 84.56, 30.60, 21.67, 21.06, 18.29; UV-Vis {Acetonitrile, λ_{max} nm ($\varepsilon/10^{-4}$ $M^{-1}cm^{-1}$)}: 263 (1.80), 302 (1.19), 346 (1.18), 462 (0.36); Anal. Calc for $C_{25}H_{25}ClN_3F_6PRu$ (648.97): C, 46.27; H, 3.88; N, 6.47. Found: C, 46.39; H, 3.95; N, 6.63%.

2.6.2. [(Benzene)Ru(L1)Cl]PF_6 (2)

Red solid, Yield: 43.8 mg (74%); IR (KBr, cm^{-1}): 3102(m), 3033(m), 1592(m), 1568(w), 1461(m), 1438(m), 838(s); ^{1}H NMR (400 MHz, DMSO-d_6, ppm): 9.57 (s, 1H) 8.94 (d, 1H, $J = 8$ Hz), 8.86 (d, 1H, $J = 8$ Hz), 8.75 (d, 1H, $J = 4$ Hz), 8.51 (d, 1H, $J = 8$ Hz), 8.32 (d, 1H, $J = 12$ Hz), 8.15–8.21 (m, 3H), 8.02 (t, 1H, $J = 8$ Hz), 7.71 (t, 1H, $J = 8$ Hz), 6.10 (s, 6H, $CH_{(benzene)}$); ^{13}C NMR (100 MHz, DMSO-d_6, ppm): 168.74, 159.68, 155.41, 148.76, 148.63, 140.74, 139.38, 133.20, 130.22, 129.50, 129.07, 128.96, 125.58, 124.99, 119.76, 87.50; UV-Vis {Acetonitrile, λ_{max} nm ($\varepsilon/10^{-4}$ $M^{-1}cm^{-1}$)}: 263 (2.54), 302 (1.97), 346 (1.98), 450 (0.57); HRMS-APCI (m/z): 448.0139 $[M\text{-}PF_6]^+$; Anal. Calc. for $C_{21}H_{17}ClN_3F_6PRu$ (592.86): C, 42.54; H, 2.89; N, 7.09. Found: C, 42.68; H, 2.81; N, 7.18%.

2.6.3. [Cp*Rh(L1)Cl]PF_6 (3)

Brown powder, Yield 46.9 mg (72%); IR (KBr, cm^{-1}): 3368(m), 2924(m), 1590(m), 1567(m), 1460(m), 1436(w), 845(s); ^{1}H NMR (400 MHz, $CDCl_3$, ppm): 9.27 (s, 1H, $CH_{(imine)}$), 8.69 (t, 2H, $J = 8$ Hz), 8.61 (d, 2H, $J = 8$ Hz), 8.28 (d, 1H, $J = 4$ Hz), 8.14 (d, 1H, $J = 12$ Hz), 7.97–8.07 (m, 2H), 7.91 (t, 1H, $J = 8$ Hz), 7.53–7.56 (m, 1H), 1.43 (s, 15H, $CH_{(Cp^*)}$); ^{13}C NMR (100 MHz, $CDCl_3$, ppm): 168.23, 158.51, 156.41, 148.28, 147.63, 140.63, 138.36, 134.20, 131.42, 129.71, 129.18, 128.35, 125.17, 122.28, 119.57, 87.38, 8.23; UV-Vis {Acetonitrile, λ_{max} nm ($\varepsilon/10^{-4}$ $M^{-1}cm^{-1}$)}: 262 (1.54), 292 (0.95), 347

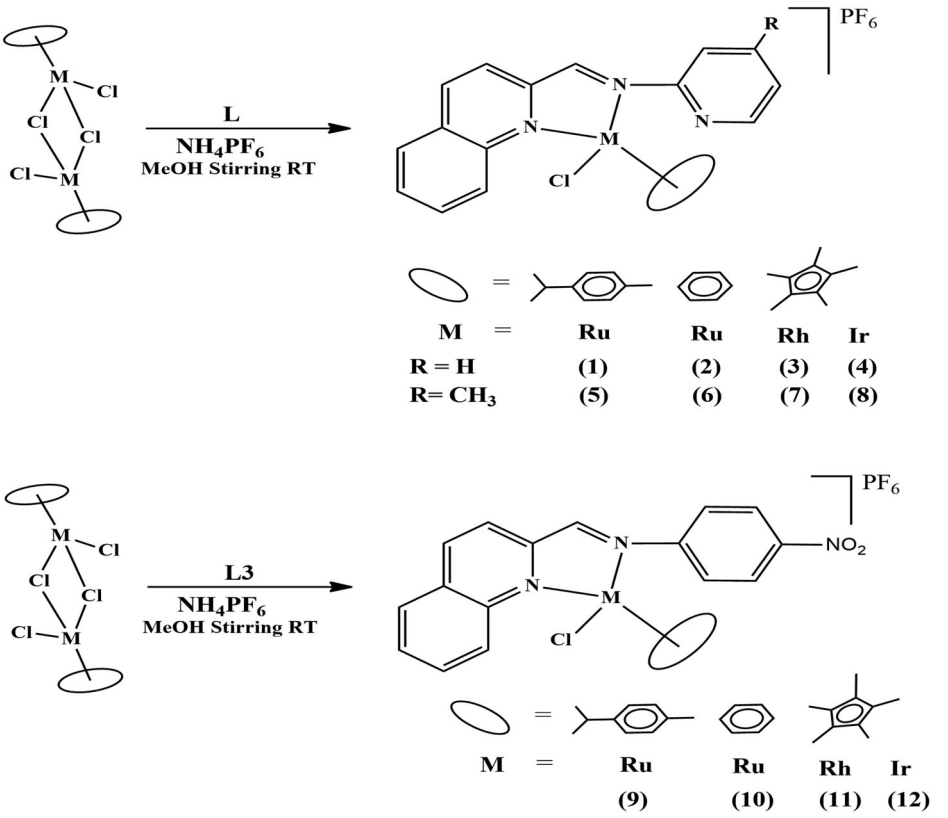

Scheme 2. Synthesis of metal complexes **1**–**12**.

(0.85), 409 (0.38); HRMS-APCI (m/z): 506.0846 $[M\text{-}PF_6]^+$; Anal. Calc for $C_{25}H_{26}ClN_3F_6PRh$ (651.81): C, 46.07; H, 4.02; N, 6.45. Found: C, 46.14; H, 4.11; N, 6.58%.

2.6.4. $[Cp^*Ir(L1)Cl]PF_6$ (4)

Brown powder, Yield 51.1 mg (69%); IR (KBr, cm^{-1}): 3135(m), 1590(m), 1563(m), 1468(w), 1436(m), 844(s); ^1H NMR (400 MHz, $CDCl_3$, ppm): 9.61 (s, 1H, $CH_{(imine)}$), 8.70 (t, 1H, $J = 4$ Hz), 8.66 (d, 1H, $J = 8$ Hz), 8.57 (d, 1H, $J = 8$ Hz), 8.42 (d, 1H, $J = 8$ Hz), 8.23 (d, 1H, $J = 8$ Hz), 8.13 (d, 1H, $J = 8$ Hz), 7.99 (t, 2H, $J = 8$ Hz), 7.91 (t, 1H, $J = 8$ Hz), 7.53–7.56 (m, 1H), 1.45 (s, 15H, CH_{Cp^*}); ^{13}C NMR (100 MHz, $CDCl_3$, ppm): 167.15, 159.54, 157.33, 149.28, 146.13, 139.25, 138.36, 135.75, 130.42, 129.88, 129.08, 128.23, 126.48, 123.65, 119.13, 86.16, 8.07; UV-Vis {Acetonitrile, λ_{max} nm ($\varepsilon/10^{-4}$ $M^{-1}cm^{-1}$)}: 264 (1.37), 312 (0.83), 348 (0.88), 428 (0.28); HRMS-APCI (m/z): 596.1563 $[M\text{-}PF_6]^+$; Anal. Calc for $C_{25}H_{26}ClN_3F_6PIr$ (741.12): C, 40.51; H, 3.54; N, 5.67. Found: C, 40.72; H, 3.62; N, 5.76%.

2.6.5. $[(P\text{-cymene})Ru(L2)Cl]PF_6$ (5)

Brown solid, Yield 48.3 mg (73%); IR (KBr, cm^{-1}): 2967(w), 1606(m), 1513(m), 1469(w), 1407(m), 843(s); ^1H NMR (400 MHz, $CDCl_3$, ppm): 9.41 (s, 1H, $CH_{(imine)}$), 7.99 (s, 1H), 7.85 (d, 3H, $J = 8$ Hz), 7.35 (d, 2H, $J = 8$ Hz), 6.89 (s, 2H), 6.67 (s, 1H), 5.49 (d, 2H, $J = 4$ Hz, $CH_{(p\text{-cym})}$), 5.36 (d, 2H, $J = 4$ Hz, $CH_{(p\text{-cym})}$), 2.87–2.98 (sept, 1H, $CH_{(p\text{-cym})}$), 2.43 (s, 3H), 2.16 (s, 3H, $CH_{(p\text{-cym})}$), 1.28 (d, 6H, $J = 8$ Hz, $CH_{(p\text{-cym})}$); ^{13}C NMR (100 MHz, $CDCl_3$, ppm):

167.17, 160.70, 157.43, 154.86, 151.68, 148.83, 141.02, 134.01, 131.10, 129.80, 129.42, 128.77, 126.98, 124.81, 119.49, 86.32, 86.09, 86.03, 85.45, 31.20, 22.29, 21.39, 18.69, 14.00; UV-Vis {Acetonitrile, λ_{max} nm ($\varepsilon/10^{-4}$ $M^{-1}cm^{-1}$)}: 262 (0.451), 396 (0.128); Anal. Calc for $C_{26}H_{27}ClN_3RuF_6P$ (663.00): C, 47.10; H, 4.10; N, 6.34. Found: C, 47.18; H, 4.06; N, 6.41%.

2.6.6. [(Benzene)Ru(L2)Cl]PF_6 (6)

Yellow solid, Yield 42.4 mg (70%); IR (KBr, cm^{-1}): 2966(m), 1605(m), 1536(m), 1469(m), 1439(m), 842(s); ^{1}H NMR (400 MHz, $CDCl_3$, ppm): 9.54 (s, 1H), 8.38 (s, 2H), 7.88 (d, 1H, $J = 8$ Hz), 7.67 (d, 2H, $J = 12$ Hz), 7.57 (d, 1H, $J = 4$ Hz), 7.00 (d, 2H, $J = 8$ Hz), 6.48 (s, 1H), 6.09 (s, 6H, $CH_{(benzene)}$), 2.44 (s, 6H); UV-Vis {Acetonitrile, λ_{max} nm ($\varepsilon/10^{-4}$ $M^{-1}cm^{-1}$)}: 236 (0.452), 320 (0.402), 389 (0.256); Anal. Calc for $C_{22}H_{19}ClN_3F_6PRu$ (606.89): C, 43.54; H, 3.16; N, 6.92. Found: C, 43.61; H, 3.23; N, 6.97%.

2.6.7. [Cp*Rh(L2)Cl]PF_6 (7)

Yellow solid, Yield 45.2 mg (68%); IR (KBr, cm^{-1}): 3154(m), 1603(s), 1511(m), 1402(s), 842(s); ^{1}H NMR (400 MHz, $CDCl_3$, ppm): 9.78 (s, 1H, $CH_{(imine)}$), 8.21 (s, 1H), 7.98 (s, 1H), 7.84 (d, 2H, $J = 8$ Hz), 7.34 (d, 2H, $J = 8$ Hz), 6.88 (d, 2H, $J = 4$ Hz), 6.66 (s, 1H), 2.42 (s, 3H), 1.60 (s, 15H, $CH_{(Cp^*)}$); ^{13}C NMR (100 MHz, $CDCl_3$, ppm): 168.85, 161.08, 157.95, 154.14, 153.79, 152.63, 138.69, 138.35, 133.83, 130.14, 127.44, 127.18, 126.58, 125.99, 119.06, 95.97, 19.99, 7.34; UV-Vis {Acetonitrile, λ_{max} nm ($\varepsilon/10^{-4}$ $M^{-1}cm^{-1}$)}: 223 (0.762), 497 (0.125); ESI-MS (m/z): 520.119 $[M\text{-}PF_6]^+$. Anal. Calc for $C_{26}H_{28}ClN_3F_6PRh$ (665.84): C, 46.90; H, 4.24; N, 6.31. Found: C, 46.89; H, 4.29; N, 6.27%.

2.6.8. [Cp*Ir(L2)Cl]PF_6 (8)

Red solid, Yield 48.3 mg (64%); IR (KBr, cm^{-1}): 2965(m), 1604(m), 1513(m), 1456(w), 1408(m), 844(s); ^{1}H NMR (400 MHz, $CDCl_3$, ppm): 8.99 (s, 1H, $CH_{(imine)}$), 8.38 (d, 1H, $J = 8$ Hz), 8.09 (d, 1H, $J = 8$ Hz), 8.02 (d, 1H, $J = 8$ Hz), 7.80 (d, 1H, $J = 8$ Hz), 7.62 (d, 2H, $J = 8$ Hz), 7.35 (t, 1H, $J = 8$ Hz), 7.29 (d, 1H, $J = 8$ Hz), 6.51 (s, 1H), 2.39 (s, 3H), 1.53 (s, 15H, $CH_{(Cp^*)}$); ^{13}C NMR (100 MHz, DMSO-d_6, ppm): 168.88, 156.74, 153.96, 151.33, 148.90, 146.09, 142.07, 134.22, 133.59, 131.21, 129.70, 129.01, 127.00, 124.80, 120.13, 90.87, 21.95, 8.75; UV-Vis {Acetonitrile, λ_{max} nm ($\varepsilon/10^{-4}$ $M^{-1}cm^{-1}$)}: 242 (0.577), 288 (0.456), 502 (0.113); ESI-MS (m/z): 610.160 $[M\text{-}PF_6]^+$. Anal. Calc for $C_{26}H_{28}ClN_3F_6PIr$ (755.15): C, 41.35; H, 3.74; N, 5.56. Found: C, 41.72; H, 3.71; N, 5.69%.

2.6.9. [(P-cymene)Ru(L3)Cl]PF_6 (9)

Yellow solid, Yield 56.8 mg (82%); IR (KBr, cm^{-1}): 2922(m), 1642(m), 1524(s), 1347(m), 844(s); ^{1}H NMR (400 MHz, $CDCl_3$ + DMSO-d_6, ppm): 8.78 (s, 1H, $CH_{(imine)}$), 8.66 (d, 1H, J = 8 Hz), 8.56 (d, 1H, $J = 8$ Hz), 8.36 (d, 2H, $J = 8$ Hz), 8.28 (d, 1H, $J = 8$ Hz), 8.19 (d, 2H, $J = 12$ Hz), 8.04 (t, 1H, $J = 8$ Hz), 7.97 (d, 1H, $J = 8$ Hz), 7.86 (t, 1H, $J = 8$ Hz), 5.69 (d, 1H, $J = 4$ Hz, $CH_{(p\text{-}cym)}$), 5.64 (d, 1H, $J = 4$ Hz, $CH_{(p\text{-}cym)}$), 5.39 (d, 1H, $J = 4$ Hz, $CH_{(p\text{-}cym)}$), 5.20 (d, 1H, $J = 4$ Hz, $CH_{(p\text{-}cym)}$), 2.51 (sept, 1H, $CH_{(p\text{-}cym)}$), 2.03 (s, 3H), 0.78 (d, 6H); ^{13}C NMR (100 MHz, $CDCl_3$ + DMSO-d_6, ppm): 175.15, 161.32, 160.02, 152.94, 145.84, 138.58, 135.79, 134.34, 133.91, 130.14, 128.61, 117.53, 91.28, 90.75, 90.66, 89.92, 35.61, 27.15, 26.26, 23.45; UV-Vis {Acetonitrile, λ_{max} nm ($\varepsilon/10^{-4}$ $M^{-1}cm^{-1}$)}: 232 (0.217), 312 (0.196),

496 (0.110); ESI-MS (m/z): 548.105 $[M\text{-}PF_6]^+$. Anal. Calc for $C_{26}H_{25}ClN_3O_2RuPF_6$ (692.98): C, 45.06; H, 3.64; N, 6.06. Found: C, 45.02; H, 3.67; N, 5.99%.

2.6.10. [(Benzene)Ru(L3)Cl]PF_6 (10)

Yellow solid, Yield 41.3 mg (65%); IR (KBr, cm^{-1}): 2926(m), 1637(w), 1525(s), 1461(w), 1384(s), 851(s); ^1H NMR (400 MHz, $CDCl_3$, ppm): 9.25 (s, 1H), 8.85 (t, 2H, $J = 8$ Hz), 8.49 (d, 2H, $J = 4$ Hz), 8.27 (d, 3H, $J = 4$ Hz), 8.19 (s, 1H) 8.00 (d, 1H, $J = 4$ Hz), 7.93 (d, 1H, $J = 4$ Hz), 5.99 (s, 6H, $CH_{(benzene)}$); ^{13}C NMR (100 MHz, $CDCl_3$ + DMSO-d_6, ppm): 171.18, 156.66, 155.88, 149.14, 148.11, 141.24, 133.77, 130.77, 129.60, 129.47, 125.33, 124.37, 88.14; UV-Vis {Acetonitrile, λ_{max} nm ($\varepsilon/10^{-4}$ $M^{-1}cm^{-1}$)}: 223 (0.382), 376 (0.482), 503 (0.132); Anal. Calc for $C_{22}H_{17}ClN_3O_2RuPF_6$ (636.87): C, 41.49; H, 2.69; N, 6.60. Found: C, 41.52; H, 2.73; N, 6.68%.

2.6.11. [Cp*Rh(L3)Cl]PF_6 (11)

Orange solid, Yield 55.0 mg (79%); IR (KBr, cm^{-1}): 2924(m), 1635(m), 1521(s), 1382(w), 1347(s), 841(s); ^1H NMR (400 MHz, $CDCl_3$, ppm): 9.03 (s, 1H, $CH_{(imine)}$), 8.73 (d, 1H, $J = 8$ Hz), 8.53 (d, 1H, $J = 8$ Hz), 8.46 (d, 2H, $J = 8$ Hz), 8.41 (d, 1H, $J = 8$ Hz), 8.30 (d, 2H, $J = 8$ Hz), 8.16 (d, 1H, $J = 8$ Hz), 8.07 (t, 1H, $J = 8$ Hz), 7.93 (t, 1H, $J = 8$ Hz), 1.43 (s, 15H, $CH_{(Cp^*)}$); ^{13}C NMR (100 MHz, $CDCl_3$ + DMSO-d_6, ppm): 169.36, 153.17, 151.99, 147.11, 145.72, 140.52, 132.16, 130.09, 128.59, 128.10, 124.38, 123.44, 97.25, 8.16; UV-Vis {Acetonitrile, λ_{max} nm ($\varepsilon/10^{-4}$ $M^{-1}cm^{-1}$)}: 318(0.789), 512 (0.214); ESI-MS (m/z): 550.078 $[M\text{-}PF_6]^+$. Anal. Calc for $C_{26}H_{26}ClN_3O_2RhPF_6$ (695.82): C, 44.88; H, 3.77; N, 6.04. Found: C, 44.90; H, 3.81; N, 6.03%.

2.6.12. [Cp*Ir(L3)Cl]PF_6 (12)

Orange solid, Yield 49.2 mg (65%); IR (KBr, cm^{-1}): 2938(m), 1634(m), 1522(s), 1406(w), 1352(s), 844(s); ^1H NMR (400 MHz, $CDCl_3$, ppm): 9.75 (s, 1H, $CH_{(imine)}$), 8.82 (d, 2H, $J = 8$ Hz), 8.49 (d, 3H, $J = 8$ Hz), 8.24 (d, 3H, $J = 8$ Hz), 8.11 (t, 1H, $J = 4$ Hz), 7.99 (t, 1H, $J = 8$ Hz), 1.43 (s, 15H, $CH_{(Cp^*)}$); ^{13}C NMR (100 MHz, $CDCl_3$ + DMSO-d_6, ppm): 170.72, 153.58, 145.69, 140.83, 133.46, 132.30, 130.24, 129.16, 128.68, 127.08, 124.92, 120.56, 97.73, 8.57; UV-Vis {Acetonitrile, λ_{max} nm ($\varepsilon/10^{-4}$ $M^{-1}cm^{-1}$)}: 220 (0.421), 352 (0.423), 521 (0.231); ESI-MS (m/z): 640.134 $[M\text{-}PF_6]^+$. Anal. Calc for $C_{26}H_{26}ClN_3O_2IrPF_6$ (785.13): C, 39.77; H, 3.34; N, 5.35. Found: C, 39.83; H, 3.41; N, 5.39%.

3. Results and discussion

3.1. Synthesis of complexes

Metal complexes **1**–**12** were synthesized by the reaction of metal precursors with an imino-quinolyl ligand in methanol. The complexes were isolated as cationic salts with PF_6^- counter ions. All these metal complexes were obtained in good yields and are yellow, red or brown in color. They are stable in air as well as in the solid state, and are non-hygroscopic. These complexes are soluble in common organic solvents such as dichloromethane, acetonitrile, acetone and DMSO, but insoluble in diethyl ether and hexane. The metal complexes were fully characterized by spectroscopic

techniques. The molecular structures of some of the complexes were established by single crystal X-ray analysis.

3.2. Spectroscopic characterization of imino-quinolyl metal complexes

3.2.1. Ir studies of metal complexes

In the IR spectra of the metal complexes the C = N stretching frequencies were detected in lower frequency region around 1563–1592 cm^{-1} which suggest coordination of the imino-quinolyl ligand occurs through the imine and quinoline nitrogen atoms. A strong band is also observed in the spectra of **9**–**12** in the region 1521–1525 cm^{-1}, corresponding to the asymmetric stretching vibration of N-O. All the metal complexes displayed a sharp band around 838–851 cm^{-1} corresponding to the P-F stretching frequency of the counter ion [28].

3.2.2. ^{1}H NMR studies of metal complexes

The proton NMR spectra of the metal complexes further confirm formation of the complexes. In the metal complexes, the signals associated with the ligand protons were observed in the downfield region as compared to the free ligand which suggests the coordination of the imino-quinolyl ligand to the metal ion. The aromatic proton signals were observed in the range 6.51–8.94 ppm. The imine proton signal was observed in the downfield region 8.98–9.78 ppm as compared to the free ligand at 8.06 ppm, which indicates the coordination of the imine bond to the metal center. The aromatic protons of the *p*-cymene ligand of **1**, **5** and **9** are doublets in the range 5.20–5.69 ppm. The isopropyl group of the *p*-cymene ligand was observed as doublets around 1.28–0.73 ppm, the methyl protons of the *p*-cymene ligand were observed as a singlet and methine protons of the *p*-cymene ligand were observed as a heptet. This splitting pattern of *p*-cymene ligand protons is due to the desymmetrization of the *p*-cymene moiety upon coordination of the imino-quinolyl ligand, which correlates well with our previous reported complexes [29]. The aromatic protons of the benzene ruthenium complexes **2**, **6** and **10** displayed singlets at 6.10, 6.09 and 5.99 ppm, respectively, corresponding to the six protons of the benzene ring. The Cp*Rh and Cp*Ir complexes **3**, **4**, **7**, **8**, **11** and **12** exhibited singlets at 1.43, 1.45, 1.60, 1.53, 1.43 and 1.43 ppm, respectively, corresponding to the methyl protons of the Cp* group. Thus, the proton NMR spectra of the complexes strongly support the formation of the metal complexes.

3.2.3. ^{13}C NMR studies of the metal complexes

Further confirmation of the formation of complexes was established by measuring the ^{13}C NMR spectra of the complexes. The carbon resonances associated with the ligand were observed in the downfield region 118 to 175 ppm. In **1**, **5** and **9** the aromatic carbon signals for the *p*-cymene ligand were observed in the region 84–109 ppm while the methine, methyl and isopropyl carbon resonances were observed in the region 18–31 ppm. Complexes **2** and **10** displayed sharp signals at 87.50 and 88.14 ppm for the carbon of benzene ring. The ring carbons of the Cp* ligand for **3**, **4**, **7**, **8**, **11** and

12 were observed around 97.73–86.16 ppm and the signal for methyl carbons of Cp* was observed in the range 8.75–7.34 ppm.

3.2.4. Electronic spectra of metal complexes

The electronic spectra of the imino-quinolyl metal complexes were recorded in acetonitrile solution at room temperature and the respective plots are shown in supporting information Figures S20 and S21. These complexes displayed three absorption bands in the region around 225–500 nm. The band in the higher energy region around 225–320 nm and 300–350 nm can be assigned as ligand centered π-π* and n-π* transition. The low oxidation state d^6 metal complexes provide filled dπ (t_{2g}) orbitals, which can interact with low-lying π* orbitals of the imino-quinolyl ligand and therefore one can expect a metal to ligand (MLCT) charge transfer band. The broad absorption band in the visible region around 405–500 nm has been attributed as metal to ligand charge transfer (MLCT) band arising from M (dπ) to π* (ligand) transition.

The m/z values of the representative complexes are listed in the Experimental section and are presented in the Supporting Information, supporting information Figures S22–S29. Complexes **2**, **3**, **4**, **7**, **8**, **9**, **11** and **12** display predominant peaks at m/z 448.0139, 506.0846, 596.1563, 520.119, 610.160, 548.105, 550.078 and 640.134, respectively, corresponding to $[M\text{-}PF_6]^+$ ion peak.

3.3. Description of the crystal structures of complexes

In addition to the spectroscopic analysis, we were also able to establish the molecular structures of some of **1**, **2** and **4**. The methyl groups of Cp* in **4** are disordered resulting in the methyl groups having large thermal ellipsoids. Complex **4**'s crystal structure is presented to only confirm the composition of molecule. Single crystal X-ray diffraction analysis was carried out to confirm the coordination of the imino-quinolyl ligand to the metal ion and to understand the geometry of the complexes. Thermal ellipsoid plots of the complexes along with the atom numbering scheme are shown in Figures 1 and 2, respectively. The detailed summary of the crystal data including data collection and structure refinement parameters are summarized in Table 1 and selected bond lengths and angles, including those involving the metal ion and ring centroids, are listed in Table 2. Complex **1** crystallized in the triclinic system with space group *P 1* and **2** crystallized in the monoclinic crystal system with space group $P2_1/c$.

All these complexes have a cationic species with the general formula [(arene)M(L)Cl] with counter-ion PF_6^-. These complexes adopt a typical three-legged piano-stool geometry (a description commonly employed for half-sandwich complexes) around the metal center with coordination sites occupied by an arene ring (arene = *p*-cymene and benzene) in a η^6 manner, two nitrogen donor atoms from an imino-quinolyl ligand in a chelating bidentate κ^2 NN′ fashion and a terminal chloride ion. The coordination around the metal center is pseudo-octahedral wherein the arene ligand forms the seat and imino-quinolyl ligand and terminal chloride forms the legs, thus satisfying a pseudo-octahedral arrangement. The imino-quinolyl ligand coordinates to the metal center through quinolyl nitrogen N(1) and imine nitrogen (N2) in a bidentate chelating manner, thus forming a five-membered chelate ring (Figures 1 and 2). The pyridine nitrogen N(3) is not involved

in coordination. The distances between the metal and centroid of the arene ring (arene = *p*-cymene and benzene) are 1.695 (**1**) and 1.688 (**2**) Å. The Ru-N(1) bond lengths from the quinoline {2.188(4) (**1**) and 2.127(3) (**2**) Å} are comparatively longer than the imine nitrogen-metal N(2)-Ru distances {2.085(4) (**1**) and 2.075(3) (**2**) Å}. The observed Ru-N and Ru-Cl bond lengths in these imino-quinolyl complexes are in close agreement with similarly reported complexes with Schiff-base ligands [30]. The bond angle values N-Ru-Cl are close to 90° and are consistent with the piano-stool arrangement of the various group about the metal center (Table 2).

3.4. Antibacterial activity

The antibacterial potential of ligands and **1**–**12** were evaluated *in vitro* against three tested organisms: Gram-positive *S. aureus*, Gram-negative *Escherichia coli* and *Klebsiella pneumoniae* strains. The results in terms of zone of inhibition (mm) are compared with the activity of the standards ciprofloxacin (positive control). Inhibition results are measured to the nearest millimeter, which is tabulated in supporting information Table S1. The histogram of the zone of inhibition is presented in Figure 3.

The antibacterial activity of the starting metal precursors of $[(p\text{-cymene})RuCl_2]_2$, $[(benzene)RuCl_2]_2$, $[Cp^*RhCl_2]_2$ and $[Cp^*IrCl_2]_2$ were found to be inactive as previously reported [31]. All the complexes displayed effective antibacterial activity against all the studied bacterial strains, but *p*-cymene ruthenium chelates have high antibacterial activity. The slightly better activity for some metal chelates compared to the free ligands can be elucidated on the basis of chelation theory [32]. *In vitro* assay results revealed that ligands and complexes were more active against the Gram-negative bacteria than against the Gram-positive bacterium. The variance in the effectiveness of the complexes against the tested organisms is based on the difference in the cell wall structure of the Gram-negative and Gram-positive bacteria, ribosome of the microbial cells or impermeability of the cells of microbes [33]. A Gram-negative bacterium has a thin peptidoglycan layer and an outer membrane that contains proteins, lipopolysaccharide, and phospholipids, while a Gram-positive bacterium has a thick peptidoglycan layer that contains lipoteichoic acid. Hence, the cell wall of a Gram-negative bacterium is more polar, and the permeation of complexes into the microorganism is enabled by this polarity. Therefore, the effectiveness of the investigated compounds against *K. pneumoniae* is greater than against *S. aureus*. Furthermore, the results show that *p*-cymene ruthenium complex **1**, complex **5**, complex **9** and Cp*rhodium complex **7** showed good activity whereas benzene ruthenium complex **2** and **6** showed the least activity compared to other complexes. The comparison of metal ion with free ligands has been made and the results are presented in Figure 4.

It is also worth comparing these results with the antibacterial activity that was determined for some of the previously prepared ruthenium complexes. In our previous study antibacterial activities of ruthenium, rhodium and iridium complex containing azine ligands were determined and showed lower activities to those obtained in our present study [34]. Comparing these results to other reported ruthenium(II) complexes the inhibition properties of these complex are better [35]. It is clear that many factors govern the antibacterial properties of ruthenium complexes (e.g. oxidation state of metal; type of ligand, etc.) and

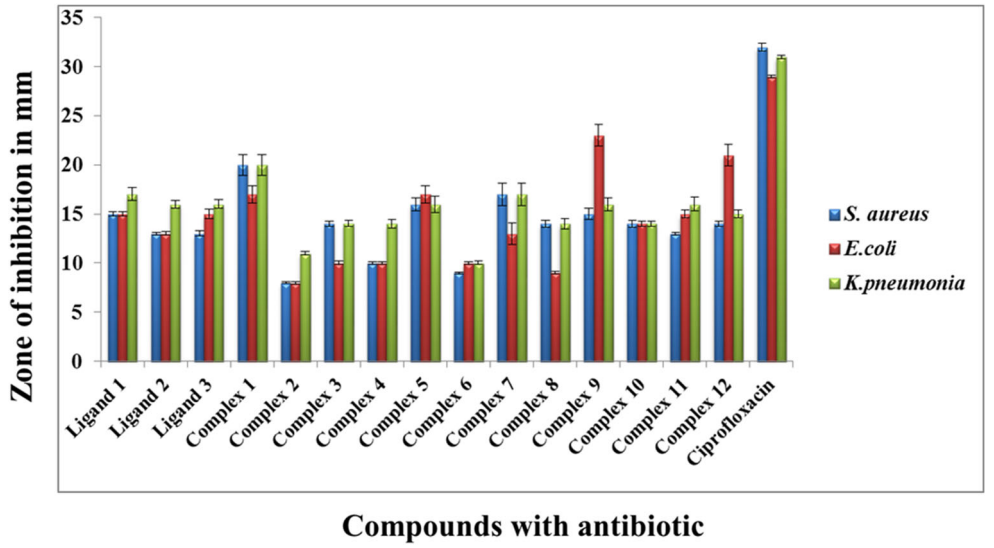

Figure 3. Histogram of the zone of inhibition (mm) of the ligands and complexes **1**–**12** in comparison with ciprofloxacin. All the complexes data are means (n = 3) ± Standard deviation of three replicates.

more research is needed to get a stronger depiction. However, the activities of all the tested complexes are less effective compared to the positive control ciprofloxacin.

3.5. MIC and MBC

The minimum inhibitory concentration (MIC) and minimum bactericidal concentration (MBC) results are listed in supporting information Table S2 and Figure 5. The MIC and MBC values of ligands and complexes **1**–**12** ranged from 0.015 to 0.5 mg/ml against all three organisms. The MIC and MBC values of **1** ranged from 0.031 to 0.062 mg/ml for *S. aureus* and *K. pneumoniae* and 0.015 to 0.031 mg/ml for *E. coli* and the values of **7** ranged from 0.062 to 0.125 mg/ml for *S. aureus* and 0.031 to 0.062 mg/ml for *E. coli* and *K. pneumoniae*. The MIC and MBC values of standard ciprofloxacin, which range from 0.031 to 0.062 mg/ml and 0.062 to 0.0125 mg/ml against the tested organisms, were taken as standards. It was found that the MBC values attained for the ligand and complexes are twice that of the corresponding MIC values. As the MBC values were twice the MIC values it can be concluded that the ligand and complexes are bacteriostatic rather than bactericidal.

4. Conclusion

We have synthesized new imino-quinolyl ligands and their corresponding ruthenium, rhodium and iridium imino-quinolyl complexes. All these complexes and ligands were fully characterized by spectroscopic analysis. These complexes were isolated as cationic salts with PF_6^- counter ion. The molecular structures of some of the complexes were established by single-crystal X-ray diffraction studies. The imino-quinolyl ligand preferably binds to the metal in a bidentate NN′ fashion using quinoline and imine

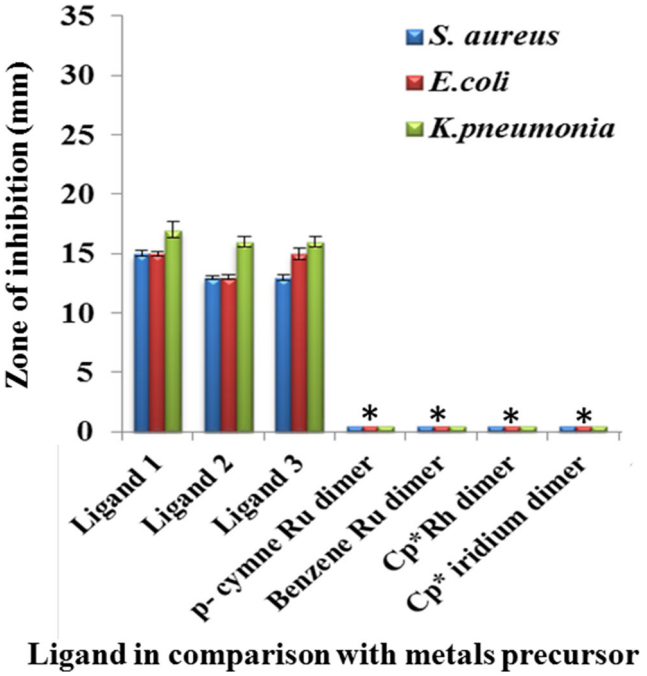

Figure 4. Histogram of the zone of inhibition (mm) of the metal ions in comparison with free ligands (where "*" indicated no zone of inhibition).

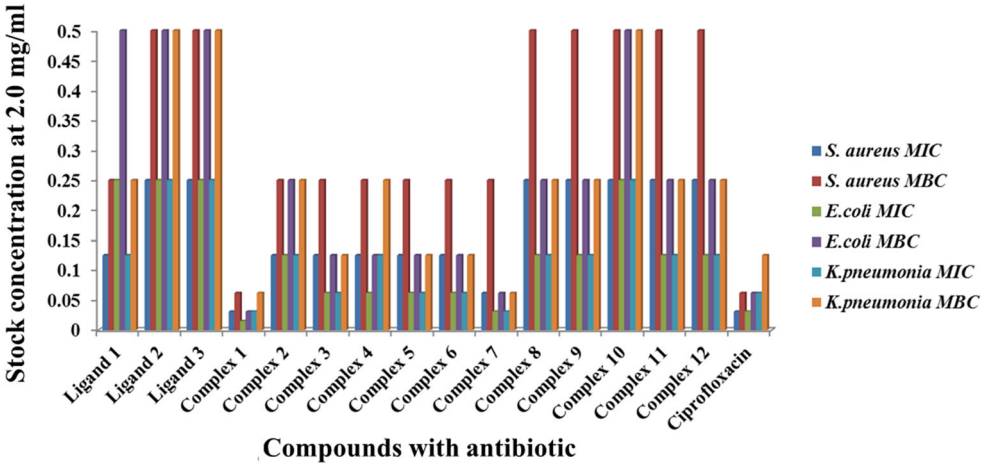

Figure 5. MIC and MBC of the ligands and complexes **1**–**12**.

nitrogen atoms forming a five-membered ring. The pyridine nitrogen N(3) is not involved in coordination to the metal center. All the compounds investigated in the present study were tested for their antibacterial properties against three strains of bacterial microorganisms, *S. aureus* (+ve), *K. pneumoniae* (-ve) and *E. coli* (-ve). The compounds showed activity against both Gram-negative bacteria and Gram-positive bacteria.

Acknowledgements

Agreeda Lapasam acknowledges the financial support of CSIR-HRDG, New Delhi in the form of SRF-NET fellowship award no. 09/347(0223)/2017-EMR-I. We thank DST-PURSE SCXRD, NEHU-SAIF, Shillong, India for providing single-crystal X-ray analysis and other spectral studies.

Disclosure statement

No potential conflict of interest was reported by the authors.

References

[1] H.W. Boucher, G.H. Talbot, J.S. Bradley, J.E. Edwards, D. Gilbert, L.B. Rice, M. Scheld, B. Spellberg, J. Bartlett. *Clin. Infect. Dis.*, **48**, 1(2009).
[2] (a) Y. Sunatsuki, Y. Motoda, N. Matsumoto. *Coord. Chem. Rev.*, **226**, 199 (2002). (b) C.M. Che, J.S. Huang. *Coord. Chem. Rev.*, **242**, 27 (2003).
[3] (a) H. Khanmohammadi, S. Amani, H. Lang, T. Rueffer. *Inorg. Chim. Acta*, **360**, 579 (2007). (b) P. DiBernardo, P.L. Zanonato, S. Tamburini, P.A. Vigato. *Inorg. Chim. Acta*, **360**, 1083 (2007).
[4] (a) R.T. Ruck, E.N. Jacobsen. *J. Am. Chem. Soc.*, **124**, 2882 (2002). (b) S. Adsule, V. Barve, D. Chen, F. Ahmed, Q.P. Dou, S. Padhye, F.H. Sarkar. *J. Med. Chem.*, **49**, 7242 (2006).
[5] (a) D.J. de Geest, A. Noble, B. Moubaraki, K.S. Murray, D.S. Larsen, S. Brooker. *Dalton Trans.*, 467 (2007). (b) U. Beckmann, S. Brooker. *Coord. Chem. Rev.*, **222**, 17 (2003). (c) S. Brooker. *Coord. Chem. Rev.*, **222**, 33 (2001).
[6] (a) M.A. Jakupec, M. Galanski, V.B. Arion, C.G. Hartinger, B.K. Keppler. *Dalton Trans.*, **2**, 183 (2008). (b) G.S. Smith, B. Therrien. *Dalton Trans.*, **40**, 10793 (2011).
[7] F. Li, J.G. Collins, F.R. Keene. *Chem. Soc. Rev.*, **44**, 2529 (2015).
[8] F. Li, Y. Mulyana, M. Feterl, J.M. Warner, J.G. Collins, F.R. Keene. *Dalton Trans.*, **40**, 5032 (2011).
[9] M. Bień, F. P. Pruchnik, A. Seniuk, T. M. Lachowicz, P. Jakimowicz. *J. Inorg. Biochem.*, **73**, 49 (1999).
[10] F. Pruchnik, D. Duś. *J. Inorg. Biochem.*, **61**, 55 (1996).
[11] (a) F. Chen, J. Moat, D. McFeely, G. Clarkson, I.J. Hands-Portman, J.P. Furner-Pardoe, F. Harrison, C.G. Dowson, P.J. Sadler. *J. Med. Chem.*, **61**, 7330 (2018). (b) A.J. Millett, A. Habtemariam, I. Romero-Canelon, G.J. Clarkson, P.J. Sadler. *Organometallics*, **34**, 2683 (2015).
[12] (a) A.M. Sugar, X. Liu, R. Chen. *Antimicrob. Agents Chemother.*, **41**, 2518 (1997). (b) A. Carta, M. Palomba, G. Paglietti, P. Molicotti, B. Paglietti, S. Cannas, S. Zanetti. *Bioorg. Med. Chem. Lett.*, **17**, 4791 (2007). (c) R.W. Winter, J.X. Kelly, M.J. Smilkstein, R. Dodean, D. Hinrichs, M.K. Riscoe. *Exp. Parasitol.*, **118**, 487 (2008).
[13] C.J. Chen, A.J. Zhang, J.B. Hu, Y.H. Miao, X. Liu. *Inorg. Chim. Acta*, **435**, 137 (2015).
[14] A. Köppl, H.G. Alt. *Alt. J. Mol. Catal. A*, **154**, 45 (2000).
[15] M. Kubanik, H. Holtkamp, T. Sohnel, S.M.F. Jamieson, C.G. Hartinger. *Organometallics*, **34**, 5658 (2015).
[16] S. Adhikari, W. Kaminsky, M.R. Kollipara. *J. Organomet. Chem.*, **836–837**, 8 (2017).
[17] S. Adhikari, W. Kaminsky, M.R. Kollipara. *J. Organomet. Chem.*, **848**, 95 (2017).
[18] D.D. Perrin, W.L.F. Armarego. *Purification of Laboratory Chemicals*, 4th Edn, Butterworths Heinemann, London (1996).
[19] (a) M.A. Bennett, T.N. Huang, T.W. Matheson, A.K. Smith, S. Ittel, W. Nickerson. *Inorg. Synth.*, **21**, 74 (1982). (b) M.A. Bennett, T.W. Matheson, G.B. Robertson, A.K. Smith, P.A. Tucker. *Inorg. Chem.*, **19**, 1014 (1980). (c) M.A. Bennett, A.K. Smith. *J. Chem. Soc., Dalton Trans.*, 233 (1974).

[20] A. Lapasam, O. Hussain, R.M. Phillips, W. Kaminsky, M.R. Kollipara. *J. Organomet. Chem.*, **880**, 272 (2019).
[21] G.M. Sheldrick. *Acta Crystallogr., Sect. A*, **71**, 3 (2015).
[22] G.M. Sheldrick. *Acta Crystallogr., Sect. C*, **71**, 3 (2015).
[23] O.D. Rigaku. *CrysAlis PRO 1.171.38.43*, Rigaku Oxford Diffraction, Yarnton (2015).
[24] L.J. Farrugia. *J. Appl. Crystallogr.*, **32**, 837 (1999).
[25] V. Banothu, A. Uma, Ch. Suvarnalaxmi, N. Chandrasekharnath, R.S. Prakasham, L. Jayalaxmi. *Curr. Trends Biotechnol. Pharm.*, **7**, 782 (2013).
[26] V. Banothu, A. Uma, J. Lingam. *Int. J. Pharm. Pharm. Sci.*, **9**, 192 (2017).
[27] V. Banothu, C. Neelagiri, A. Adepally, J. Lingam, K. Bommareddy. *Pharm. Biol.*, **55**, 1155 (2017).
[28] K. Nakamoto. *Infrared and Raman Spectra of Inorganic and Coordination Compounds, Part B*, 6th Edn, John Wiley & Sons, New Jersey (2009).
[29] S. Adhikari, N.R. Palepu, D. Sutradhar, S.L. Shepherd, R.M. Phillips, W. Kaminsky, A.K. Chandra, M.R. Kollipara. *J. Organomet. Chem.*, **820**, 70 (2016).
[30] (a) M.J. Chow, C. Licona, D.Y. Qiang Wong, G. Pastorin, C. Gaiddon, W.H. Ang. *J. Med. Chem.*, **57**, 6043 (2014). (b) H.S. Calik, E. Ispir, S. Karabuga, M. Aslantas. *J. Organomet. Chem.*, **801**, 122 (2016). (c) H. Turkmen, I. Kani, B. Cetinkaya. *Eur. J. Inorg. Chem.*, 4494 (2012). (d) S. Sangilipandi, D. Sutradhar, K. Bhattacharjee, W. Kaminsky, S.R. Joshi, A.K. Chandra, M.R. Kollipara. *Inorg. Chim. Acta*, **441**, 95 (2016).
[31] A. Lapasam, L. Dkhar, N. Joshi, K.M. Poluri, M.R. Kollipara. *Inorg. Chim. Acta*, **484**, 255 (2019).
[32] B.G. Tweedy. *Phytopathology*, **55**, 910 (1964).
[33] P.G. Lawrence, P.L. Harold, O.G. Francis. *Antibiot. Chemother.*, **4**, 1957 (1980).
[34] A. Lapasam, V. Banothu, U. Addepally, M.R. Kollipara. *J. Mol. Struct.*, **1191**, 314 (2019).
[35] P. Chuklin, V. Chalermpanaphan, T. Nhukeaw, S. Saithong, K. Chainok, S. Phongpaichit, A. Ratanaphan, N. Leesaku. *J. Organomet. Chem.*, **846**, 242(2017).